Hindawi Publishing Corporation
Advances in Materials Science and Engineering
Volume 2012, Article ID 726921, 18 pages
doi:10.1155/2012/726921

Review Article

Mn-Rich Nanostructures in $Ge_{1-x}Mn_x$: Fabrication, Microstructure, and Magnetic Properties

Ying Jiang and Yong Wang

Center of Electron Microscopy and State Key Laboratory of Silicon Materials, Department of Materials Science and Engineering, Zhejiang University, Hangzhou 310027, China

Correspondence should be addressed to Yong Wang, yongwang@zju.edu.cn

Received 22 April 2012; Accepted 18 July 2012

Academic Editor: Rupesh S. Devan

Magnetic semiconductors have attracted extensive attention due to their novel physical properties as well as the potential applications in future spintronics devices. Over the past decade, tremendous efforts have been made in the diluted magnetic semiconductors (DMS) system, with many controversies disentangled but many puzzles unsolved as well. Here in this paper, we summarize recent experimental results in the growth, microstructure and magnetic properties of Ge-based DMSs (mainly $Ge_{1-x}Mn_x$), which have been comprehensively researched owing to their compatibility with Si microelectronics. Growth conditions of high-quality, defect-free, and magnetic $Ge_{1-x}Mn_x$ bulks, thin films, ordered arrays, quantum dots, and nanowires are discussed in detail.

1. Introduction

Spin-based electronics research in the 1990s boosted with lower power consumption and greater integration comparing with the current electronics based on charge [1, 2]. Among various potential material systems, diluted magnetic semiconductors (DMSs), possessing benefits from both the charge and the spin of electrons, are considered to be most promising. In particular, Mn-doped Ge DMSs discovered in the early 2000s [3, 4] have been extensively investigated [5–8] due mainly to their compatibility with existing complementary metal-oxide-semiconductor (CMOS) technologies.

The fabrication of Ge-based DMS ($Ge_{1-x}Mn_x$) was firstly reported by Park et al. [4], with Curie temperature (T_C) increasing linearly with the Mn concentration up to 116 K for $x = 0.035$. Since then, many modified or other methods have been put forward in order to obtain a high-quality, room-temperature (RT) ferromagnetic GeMn DMS with high Mn concentration. One of the key issues to achieve ideal GeMn DMSs is to uniformly dope Mn into the Ge matrix. However, undesirable Mn-rich clusters or precipitates, such as Mn_5Ge_3 [9, 10] and $Mn_{11}Ge_8$ [7, 11], commonly occur. Although Mn_5Ge_3 and $Mn_{11}Ge_8$ phases are also ferromagnetic, both of them have metallic character, considerably hampering the discovery of intrinsic magnetic properties of the GeMn nanostructures and complicating their use as spin injectors.

The aim of this paper is to provide an overview of these efforts made on preparing differently shaped Mn-rich nanostructures in $Ge_{1-x}Mn_x$ with different preparation techniques, namely bulks by Bridgeman method and ion implantation (Section 2.1), thin films and quantum dots and ordered arrays by molecular beam epitaxy (MBE) (Sections 2.2–2.4), nanowires by thermal vapor transport method and supercritical fluid-liquid-solid method (Section 2.5), and the microstructure and magnetic properties of Ge-based DMSs under different growth conditions.

2. Growth Methods of Ge-Based (Mainly GeMn) DMSs

2.1. GeMn Bulks. In this part, we report two typical methods with which bulk GeMn DMSs can be obtained: Bridgman method and ion implantation.

2.1.1. Bridgman Method. The Bridgman method involves melting polycrystalline materials loaded in a container and

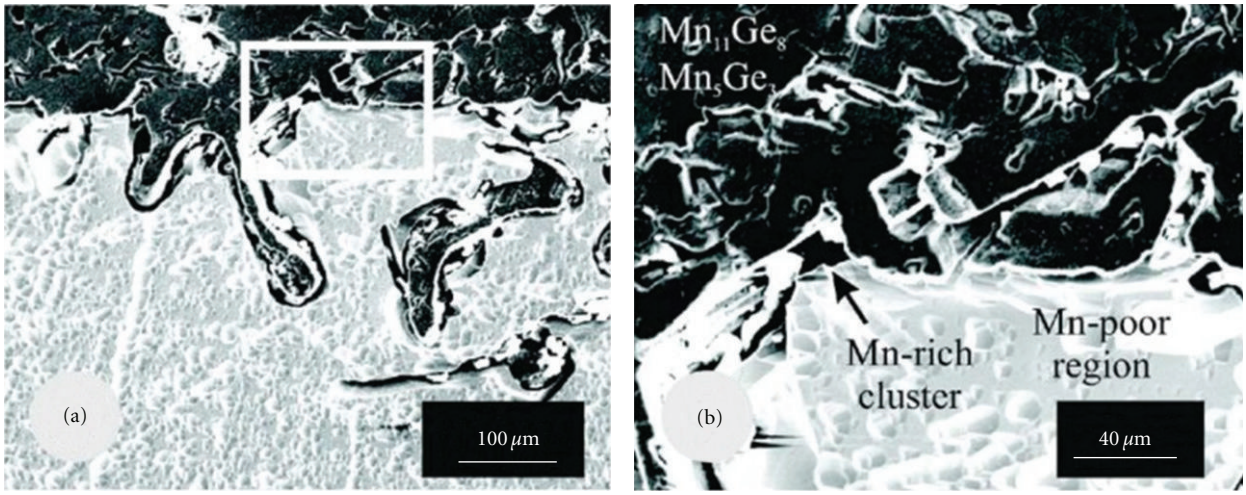

(a) (b)

Figure 1: (a) SEM image of the $Mn_{0.1}Ge_{0.9}$ crystal surface (dark regions correspond to the Mn-rich phase and bright regions to the Mn-poor phase). (b) SEM image zooming into the field marked in (a). Reproduced from [7]. Copyright ©2007, American Institute of Physics.

then slowly cooling them from one end where a seed crystal is located. The pioneering work in GeMn DMSs preparation was reported by Cho et al. [5]. High-purity germanium and manganese powders were chosen as the starting materials, and then the system was heated to 1050°C. In order to obtain single crystal, the temperature was slowly cooled at 0.5°C/h to a point below the melting temperature ~958°C for Ge and thereafter at 100°C/h. Ultimately, highly (~up to 6%) Mn-doped Ge DMS single crystals without any observable secondary phases, such as Mn_5Ge_3 and $Mn_{11}Ge_8$, were successfully fabricated with ferromagnetic order between 150 and 285 K. However, later researches have demonstrated that GeMn DMSs fabricated by this method actually consist of several Ge_xMn_y alloys, including $Mn_{11}Ge_8$ [7, 12], as shown in Figure 1 [7]. Dark regions in Figure 1 correspond to the Mn-rich phases and bright regions to the Mn-poor phases. It was found that Mn-poor phases had Mn content in the range of 1%–3%, while Mn-rich phases had the composition close to Mn_5Ge_3 and $Mn_{11}Ge_8$ phases. The magnetic behaviors in both phases indicated a homogeneous distribution of Mn-rich clusters in the Ge matrix.

2.1.2. Ion Implantation. An alternative approach to fabricate GeMn bulks, proposed in recent years, is ion implantation. Mn-implanted crystalline Ge was firstly investigated with a relatively high substrate temperature (i.e., from room temperature (RT) to 300°C) to avoid amorphization. Growth parameters of ion-implanted GeMn have been systematically investigated [10, 24–27]. Figure 2 [10] shows the nanostructures in Mn-implanted crystalline Ge at various Mn doses. The images display a fine dispersion of nanometer-size particles embedded in the Ge matrix. By increasing the Mn dose, the nanoparticles turn from amorphous to crystalline (Moirè fringes appear), together with their number and size both increasing. Similar to dose, substrate temperature also decides the nanostructures. Figure 3(a) [10] reports that RT ion implanted alloys consist of a swelled layer of oxidized amorphous Ge and a deeper layer of an amorphous alloy of Mn diluted in Ge. Sample implanted at 240°C (Figure 3(b)) shows a uniform grey background with darker clusters which are demonstrated as amorphous phase precipitation with a high Mn content (up to 7%). In a slightly higher temperature (300°C), phase precipitation occurs mostly in the form of Mn rich crystalline clusters, which are in the Mn_5Ge_3 phase (Figure 3(c)). It is noteworthy that 10 nm is considered as a critical size of the transition from amorphous to crystalline phase in the Mn rich clusters.

Although perfect dilution can be achieved in a subsurface implanted layer [24], undesirable precipitation as well as porous swelled amorphous Ge layer by radiation damage are usually observed [25]. In order to avoid the damage together with clusters and precipitates mentioned above, subsequent annealing [27, 28] or ion implantation at liquid-nitrogen temperature (LNT) was come up [13]. It has been demonstrated that when the substrate temperature during the implantation is kept well below room temperature (i.e., LNT), the swelling is not observed anymore, and the implantation produces only a compact layer of amorphous Ge, shown in Figure 4 [13]. Black lines in the images are drawn to mark the edge between the Ge upper surface (above the black lines) and the cross-sectional wall (below the black lines), while white lines mark the depth of implanted layer. Moreover, with a proper Mn fluence ($\sim 2 * 10^6$ Mn/cm^2), Mn can be perfectly diluted in the amorphous Ge, and the system can exhibit single-phase ferromagnetic behaviors up to room temperature. However, when the Mn concentration is doubled, the magnetic response becomes weaker and phase separation occurs. Special attention should also be paid to the poor electrical conductivity of amorphous GeMn, which exhibits very high resistance below the Curie temperature that may hamper its use in semiconductor spintronics device applications [29]. As another improvement of ion

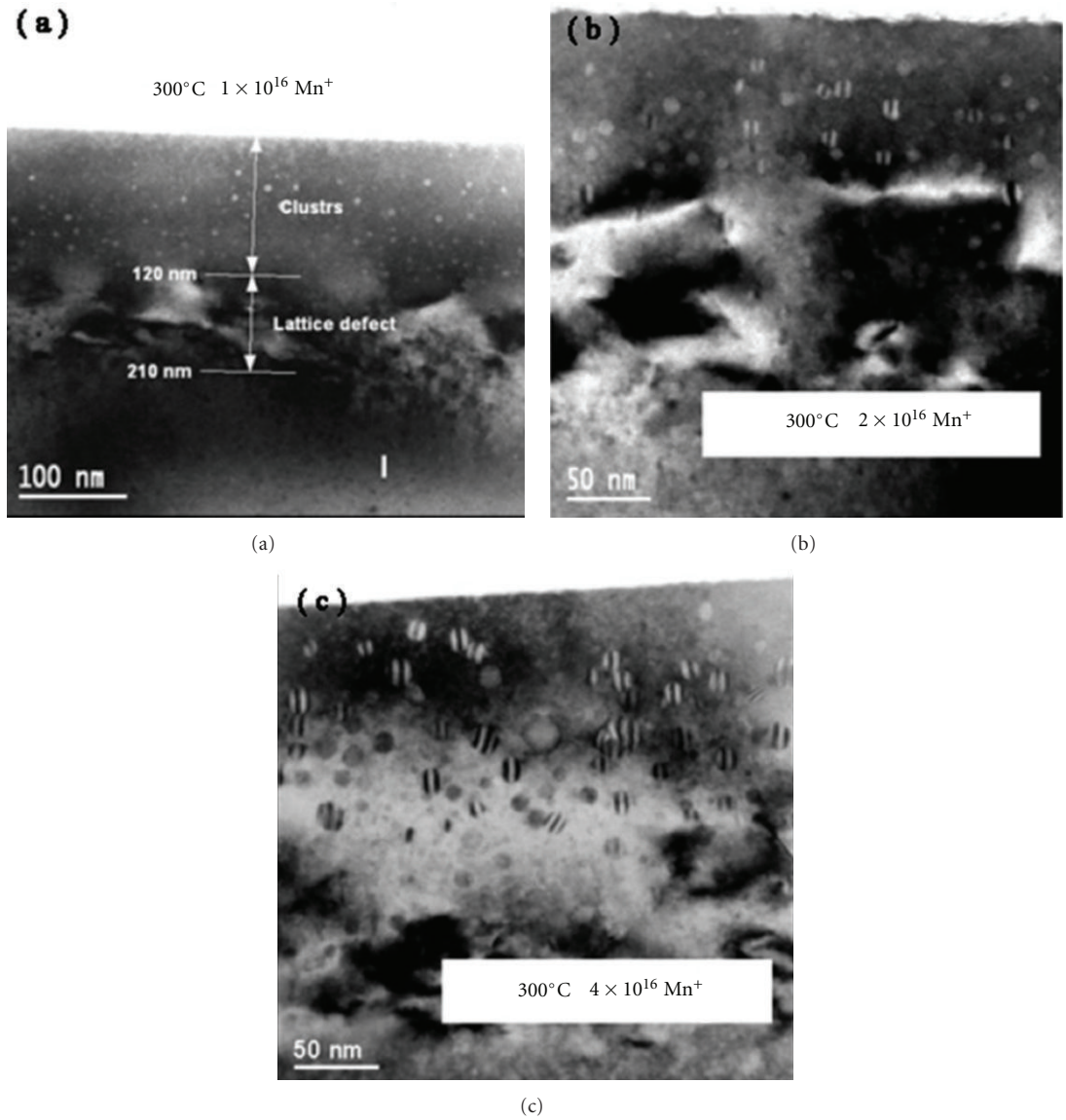

(a) (b)

(c)

Figure 2: Bright-field cross-sectional TEM images of GeMn samples implanted at various doses (same substrate temperature (T_S) of 300°C). Reproduced from [10]. Copyright ©2007, WILEY-VCH Verlag GmbH & Co. KGaA, Weinheim.

implantation, Bürger et al. [28] recently proposed a new structure called "Mn-rich Ge : Mn nanonet", which may help GeMn further develop in the application of spintronics.

2.1.3. Magnetic Properties. As the vanguard of investigation into the magnetic properties of the $Ge_{1-x}Mn_x$ bulks, Cho et al. [5] have reported that Ge alloys with low Mn concentrations show paramagnetism since the substituted Mn was separated as localized magnetic ions. At a higher concentration (~6%), Mn ions arranged in a long-range order, but magnetization did not saturate even at high magnetic fields, resulting probably from the presence of dilute (paramagnetic state) and dense (ferromagnetic state) Mn regions. Figure 5 [5] shows temperature-dependent magnetization of an $Mn_{0.04}Ge_{0.96}$ single crystal, in which the magnetization exhibits two distinct transitions at 150 and 285 K. Further study demonstrates that hysteretic behavior can be observed between the temperatures from 150 K to 285 K, indicating a ferromagnetic state. Other groups have also obtained GeMn DMSs with ion implantation with a high Curie temperature, such as 270 K [26], 293 K [13], 825 K [42]. However, the origin of the ferromagnetism was reported not all the same.

2.2. GeMn Thin Films. The major difficulty to achieve a high T_C GeMn DMS is the low solubility of Mn in the Ge matrix. A breakthrough can be made by using low-temperature molecular beam epitaxy (MBE), a thin-film growth technique in ultra-high vacuum ($< 10^{-7}$ Torr) that ensures the high quality of the films and relative high Mn

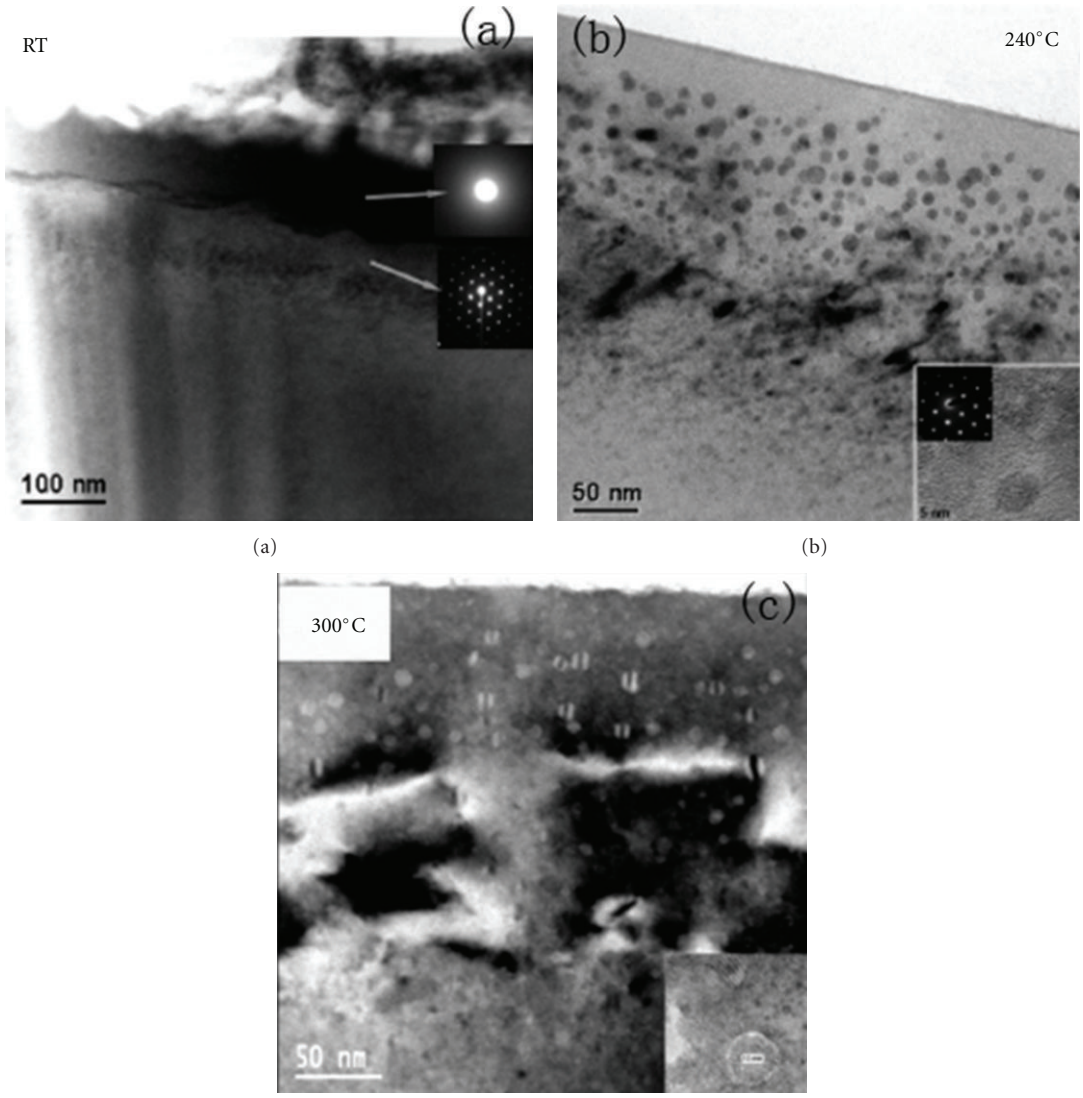

Figure 3: Bright-field cross-sectional TEM images of the GeMn samples implanted at various temperatures (same Mn dose of 2×10^{16} at./cm^2). Insets in (a): electron diffraction patterns taken in the zones marked by the arrows. Inset in (b): high resolution close-up of an amorphous nanocluster and electron diffraction pattern taken in the same zone. Inset in (c): high resolution close-up of a crystalline nanocluster. Reproduced from [10]. Copyright ©2007, WILEY-VCH Verlag GmbH & Co. KGaA, Weinheim.

solubility by working far from equilibrium. The process of MBE relates to the effects of substrates, Mn concentrations and growth temperature.

2.2.1. The Effect of Substrates. It has been predicted that Mn behavior varies on different substrates, even on the same substrate with different crystal orientations by the theoretical calculations of Zhu et al. [43]. Part of the prediction has been verified by the experimental work, which demonstrates that Mn diffuses towards the surface when the GeMn films are grown on the Si (100) substrate (Figure 6(b)) [9], but not on the Ge (100) substrate (Figure 6(a)) [11]. This phenomenon is induced by the compressive strain between Si (with a smaller lattice constant, $a = 0.543$ nm) and Ge ($a = 0.566$ nm) [9]. In order to reduce the compressive strain in Ge grown on Si, Mn atoms with a larger atom radius (140 pm) than Ge (125 pm) tend to diffuse toward the surface during the thin film growth [9]. Such Mn behavior on Si substrate leads to a higher Mn concentration in the surface region as well as formation of Mn_5Ge_3 clusters near the surface when a threshold Mn concentration is reached [9]. Fortunately, Ge buffer and low temperature during the growth can help lessen this phenomenon.

2.2.2. The Effect of Mn Concentration. It has been shown that the ferromagnetic property requires quite large Mn concentrations up to 5% [31]. Although low-temperature MBE can increase the Mn concentration by working far

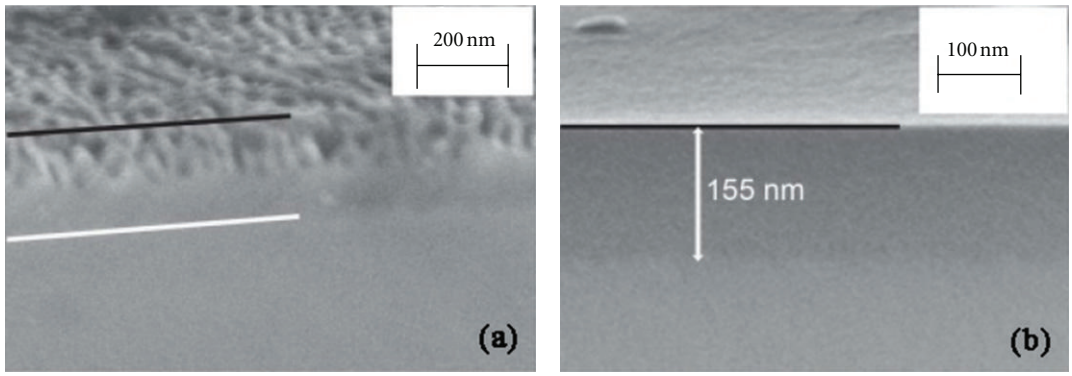

(a) (b)

Figure 4: Cross-sectional SEM images of 100 keV 2×10^{16} Mn ions/cm^2 irradiated Ge surfaces at 170°C (a) and LN substrate temperature (b). Black lines in the images are drawn to mark the edge between the Ge upper surface and the cross-sectional wall, while white lines mark the depth of implanted layer. Reproduced from [13]. Copyright ©2011, American Physical Society.

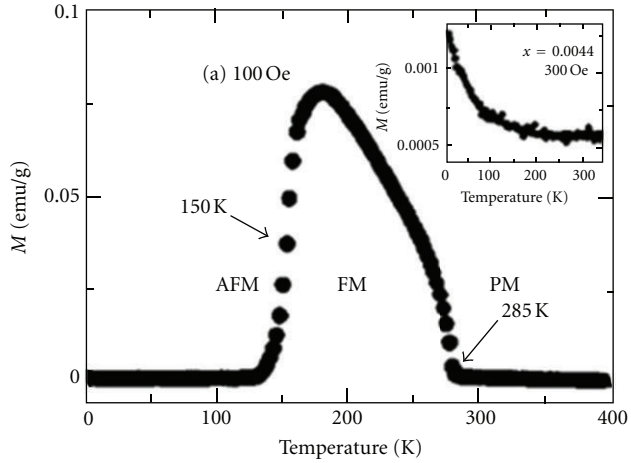

Figure 5: Magnetization versus temperature curve of $Mn_{0.04}Ge_{0.96}$ in a 100-Oe magnetic field. The inset shows paramagnetic ordering for $Ge_{1-x}Mn_x$ with $x = 0.0044$. Reproduced from [5]. Copyright ©2002, The American Physical Society.

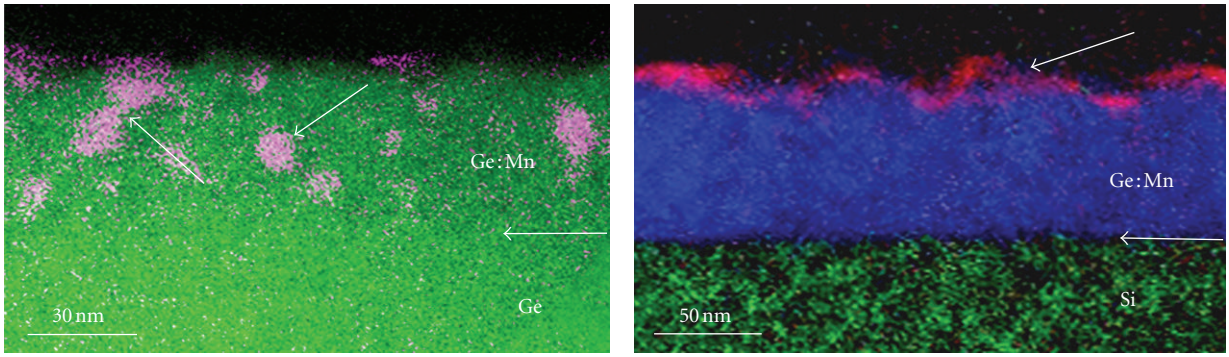

(a) (b)

Figure 6: (a) and (b) are the corresponding EELS map of GeMn films on Ge and Si, respectively. (a) Reproduced from [11]. Copyright ©2008, American Institute of Physics. (b) Reproduced from [9]. Copyright ©2008, American Institute of Physics.

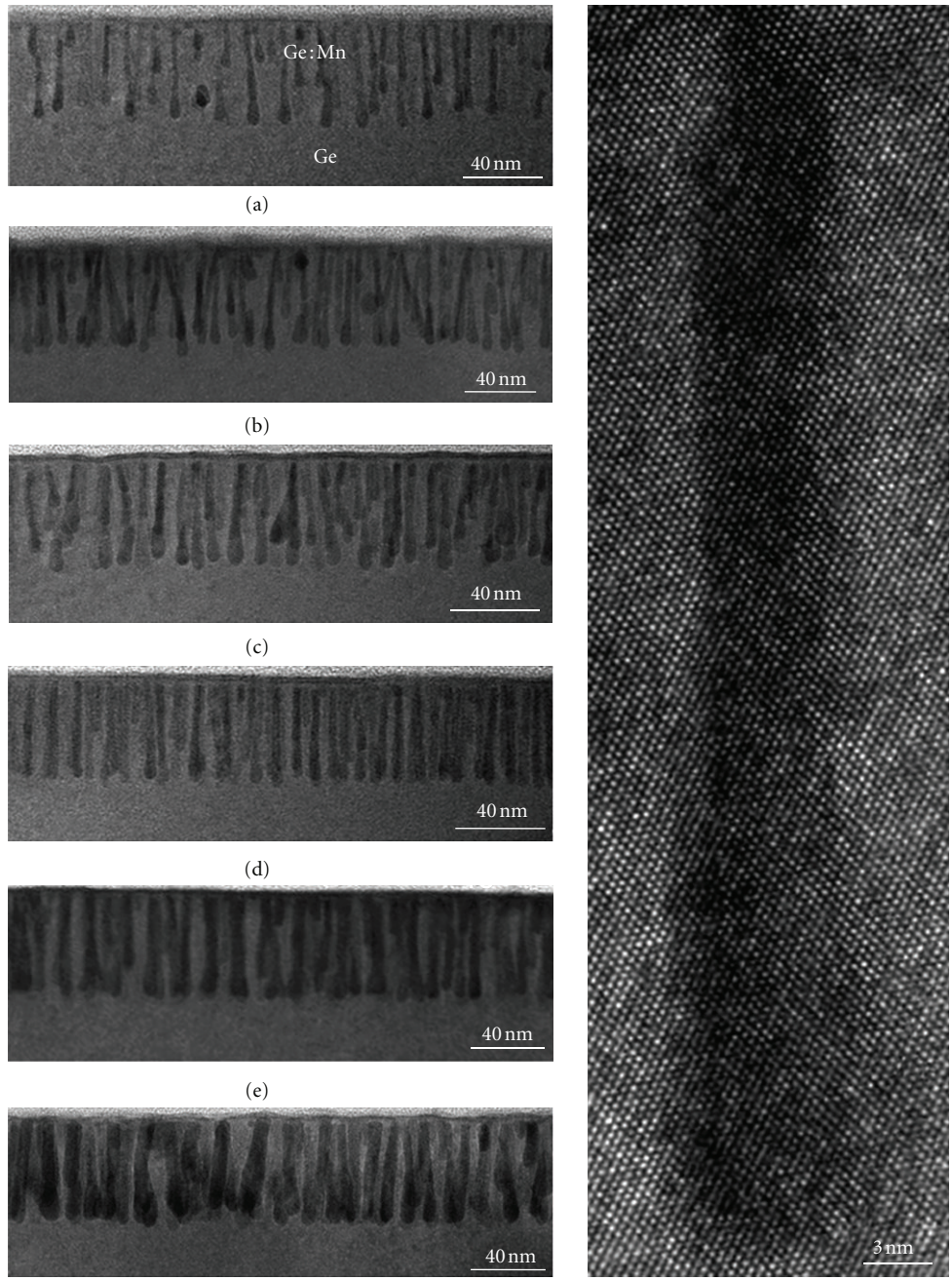

Figure 7: Cross-sectional TEM images of $Ge_{1-x}Mn_x$ grown at 70°C: (a) $x = 0.025$, (b) $x = 0.04$, (c) $x = 0.045$, (d) $x = 0.055$, (e) $x = 0.07$, (f) $x = 0.12$. (g) HRTEM image of a coherent nanocolumn. Reproduced from [14]. Copyright ©2010, Elsevier B.V..

from equilibrium, Mn tends to form clusters/precipitates when the concentration and the growth temperature reach a threshold [9]. For example, Ayoub et al. revealed Mn_5Ge_3 precipitates in diluted GeMn epitaxial films with 3.3% Mn grown by MBE [31]. In order to avoid the formation of Mn-rich clusters/precipitates and simultaneously maintain a reasonably high Mn concentration, the effect of Mn concentration on structural evolution during the film growth is essential to be systematically explored [14, 16]. Studies discover that when $Ge_{1-x}Mn_x$ thin films are grown on Si substrate at 70°C, Mn-rich tadpole-shaped clusters start to nucleate at 1% Mn and become dominant in the entire film at 4% Mn [16]. Similarly in GeMn thin films grown at 70°C on Ge substrates, by controlling the Mn concentration, the nanostructure can be manipulated. TEM images in Figure 7 [14] show the morphology of coherent Mn-rich clusters (dark contrast, Figure 7(g)) transforms from tadpoles to denser ones with longer tails (Figures 7(a)–7(c)), and eventually to nanocolumn shapes (Figure 7(d)), whose diameters continuously increase with higher Mn

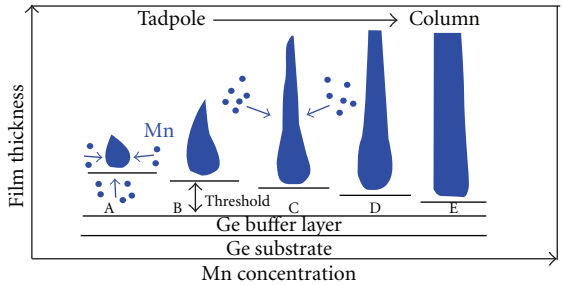

Figure 8: Schematic diagram of the structural evolution of the coherent Mn-rich clusters from tadpoles to nanocolumns in the GeMn thin films. Reproduced from [14]. Copyright ©2010, Elsevier B.V..

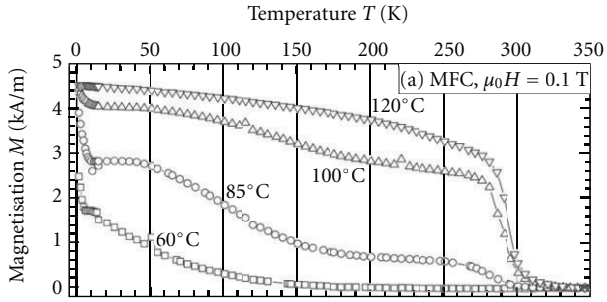

Figure 9: Temperature-dependent magnetisation of samples fabricated with substrate temperatures T_S between 60 and 120°C. Reproduced from [15]. Copyright ©2006, The American Physical Society.

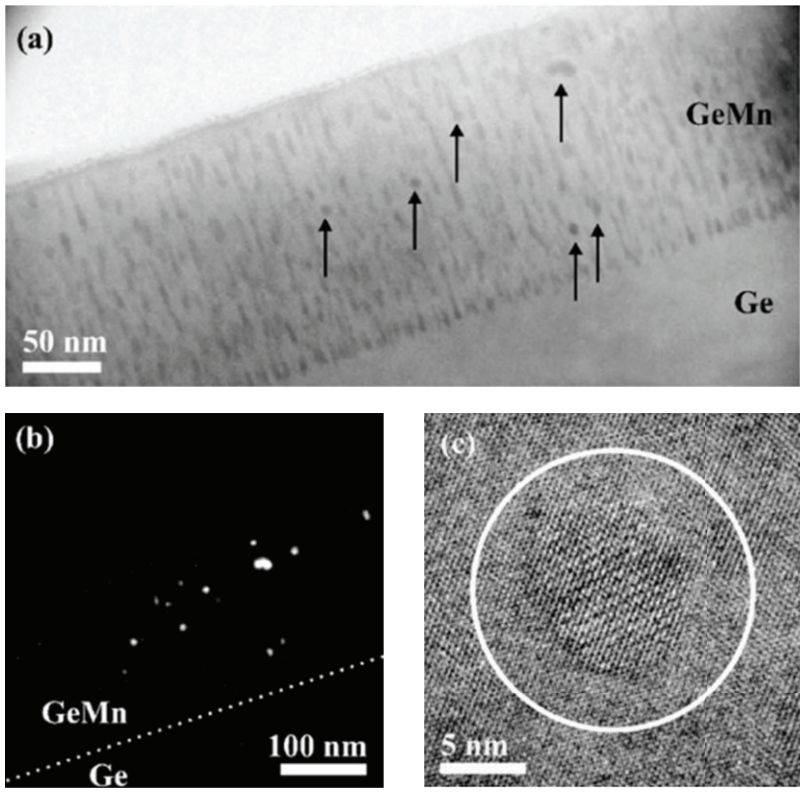

Figure 10: Cross-sectional TEM images of a sample with $T_S = 70°C$. (a) Bright-field TEM image. Mn_5Ge_3 precipitates are marked by arrows. (b) Dark-field TEM image recorded after selecting a characteristic reflex of the hexagonal Mn_5Ge_3 lattice. Bright regions indicate Mn_5Ge_3 precipitates. The dashed line is drawn to mark the interface between GeMn layer and Ge buffer layer. (c) High-resolution TEM of a typically coherent, hexagonal Mn_5Ge_3 precipitate, circled by the white line. Reproduced from [15]. Copyright ©2006, The American Physical Society.

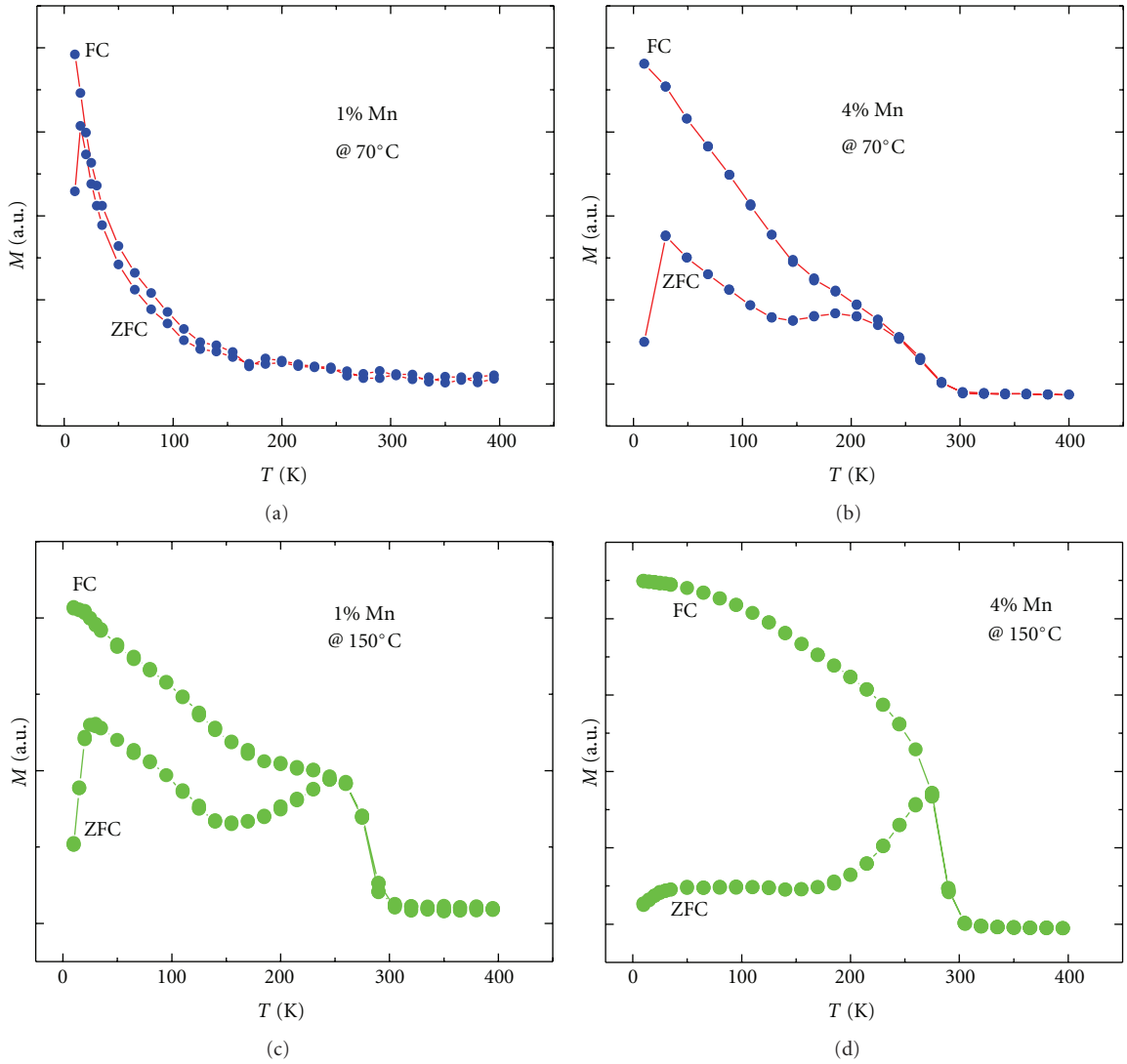

FIGURE 11: ZFC and FC curves measured with a magnetic field of 200 Oe for $Ge_{1-x}Mn_x$ samples. (a) $x = 1\%$, grown at 70°C, (b) $x = 4\%$, grown at 70°C, (c) $x = 1\%$, grown at 150°C, (d) $x = 4\%$, grown at 150°C. Reproduced from [16]. Copyright ©2010, Elsevier B.V..

concentration (Figures 7(d)–7(f)). Further study indicates that at initial growth of the GeMn thin films, Mn tends to diffuse upwards to surface. When the GeMn films reach a critical thickness (thickness threshold), Mn concentration is sufficiently high and the spinodal decomposition takes place. Based on the experimental results shown in Figure 7, a structural evolution of the coherent Mn-rich tadpoles and nanocolumns was schematized as Figure 8 [14]. It should be noted that the thickness threshold for the formation of Mn-rich clusters varies with the Mn concentration and the tendency is that the thickness threshold becomes smaller with a higher Mn concentration.

2.2.3. The Effect of Growth Temperature. GeMn thin films can achieve high-temperature ferromagnetism with a high substrate temperature T_S, as illustrated in Figure 9 [15]. However, high growth temperature can promote Mn diffusion and the formation of Mn-rich clusters/precipitates [9, 44]. Systematic study given by Li et al. [32] showed, for GeMn thin films grown on Ge with nominal 5% Mn, growth at $T_S <$ 50°C resulted in amorphous thin films. Single crystalline thin films could be obtained when T_S was between 50°C and 85°C, but with fairly low-temperature ferromagnetism indicating a possible feature for DMS. If T_S was above 85°C, the formation of Mn_5Ge_3 was observed, which had a high T_C (~296 K). Ahlers et al. [15] also investigated GeMn thin films with 5% Mn grown at 60–120°C and they found that nanosized Mn_5Ge_3 could be observed for samples grown at substrate temperature $T_S = 70$°C and precipitate-free samples could be acquired at $T_S = 60$°C, as shown in Figure 10 [15]. In addition, Jamet et al. [45] firstly reported that pure high T_C nanocolumns and a mix of nanocolumns with Mn_5Ge_3 crystallites would be obtained only when the growth temperature was between 100°C and 200°C.

2.2.4. Magnetic Properties. The magnetic properties of GeMn thin films have been extensively investigated since the first report given by Park et al. [4] demonstrated that GeMn thin

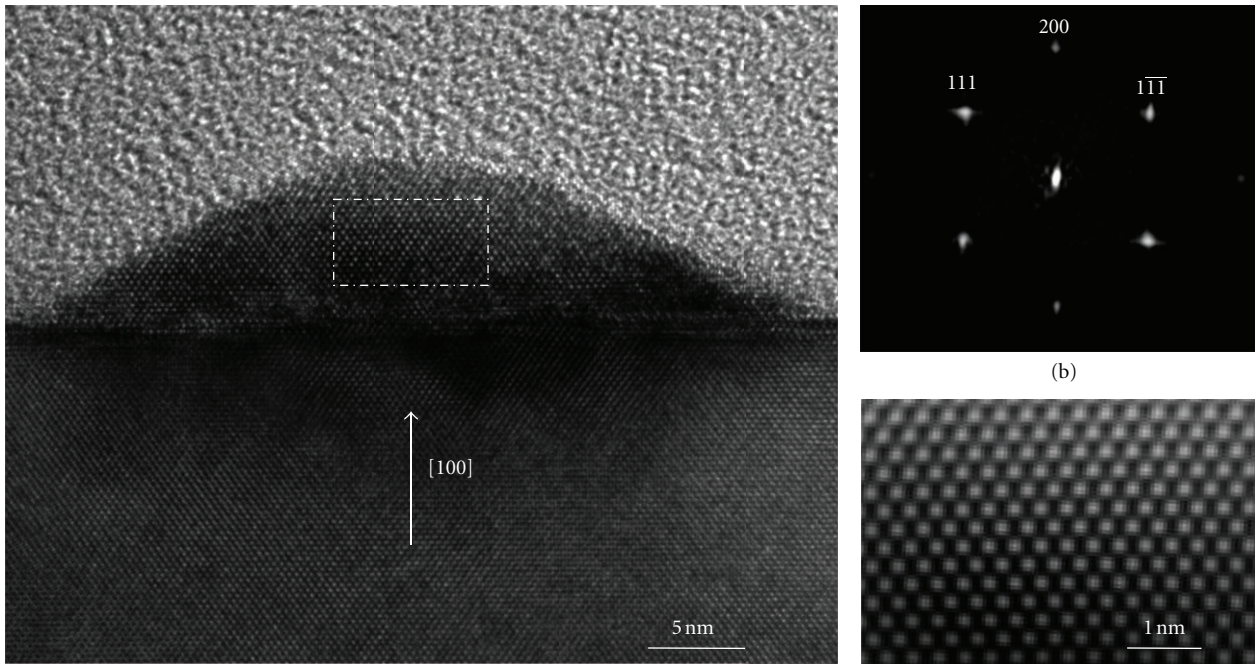

Figure 12: (a) A cross-section TEM image of a typical $Mn_{0.05}Ge_{0.95}$ QD. (b) A fast Fourier transformation (FFT). (c) A high-resolution TEM image of the MnGe lattice through the Fourier filter, showing a perfect coherence. Reproduced from [17]. Copyright ©2010, Macmillan Publishers Limited.

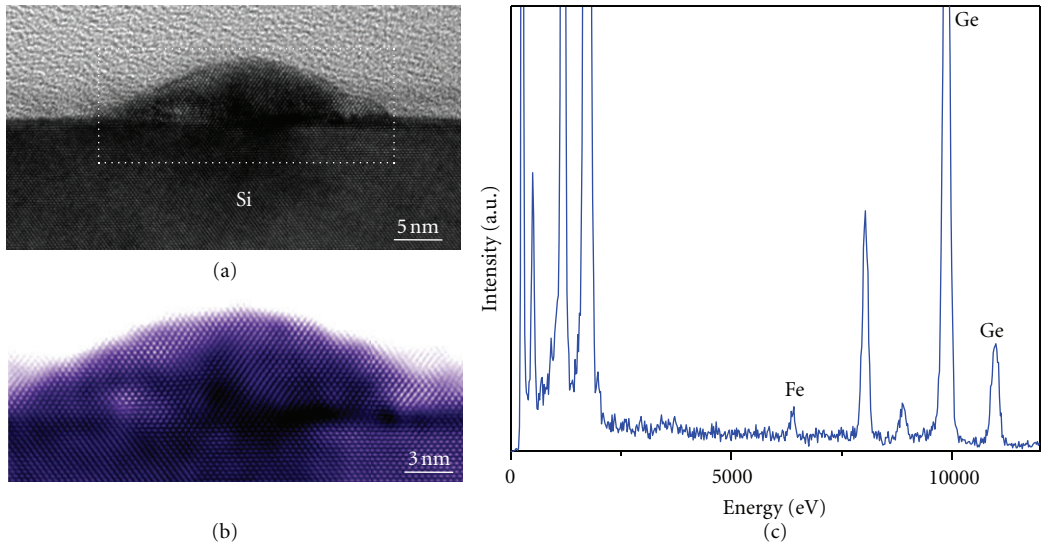

Figure 13: (a) A high-resolution TEM image of one $Fe_{0.02}Ge_{0.98}$ QD on Si. (b) A magnified Fourier-filtered image of the marked area in (a), showing nearly perfect lattice coherence between Si and QDs. (c) EDX results for Fe concentration (~2 atom%). Reproduced from [18]. Copyright ©2010, American Chemical Society.

films could achieve a T_C up to 116 K with a Mn concentration of 3.5% and the ferromagnetism was carrier mediated. Although in the recent ten years, quite high-temperature ferromagnetism has been achieved, most research results indicate the origin of room temperature T_C is associated with the Mn_5Ge_3 precipitates [15, 16, 33]. In addition, Devillers et al. [34] identified four magnetic phases with different T_C in their GeMn thin films: diluted Mn in Ge matrix, low-T_C nanocolumns ($T_C \leq 170$ K), high-T_C nanocolumns ($T_C \geq 400$ K), and Mn_5Ge_3 precipitates ($T_C \sim 300$ K).

As mentioned in Sections 2.2.2 and 2.2.3, Mn concentration, as well as substrate temperature has considerable effects on the nanostructure of GeMn thin films, consequently influencing the magnetic properties. The magnetic features

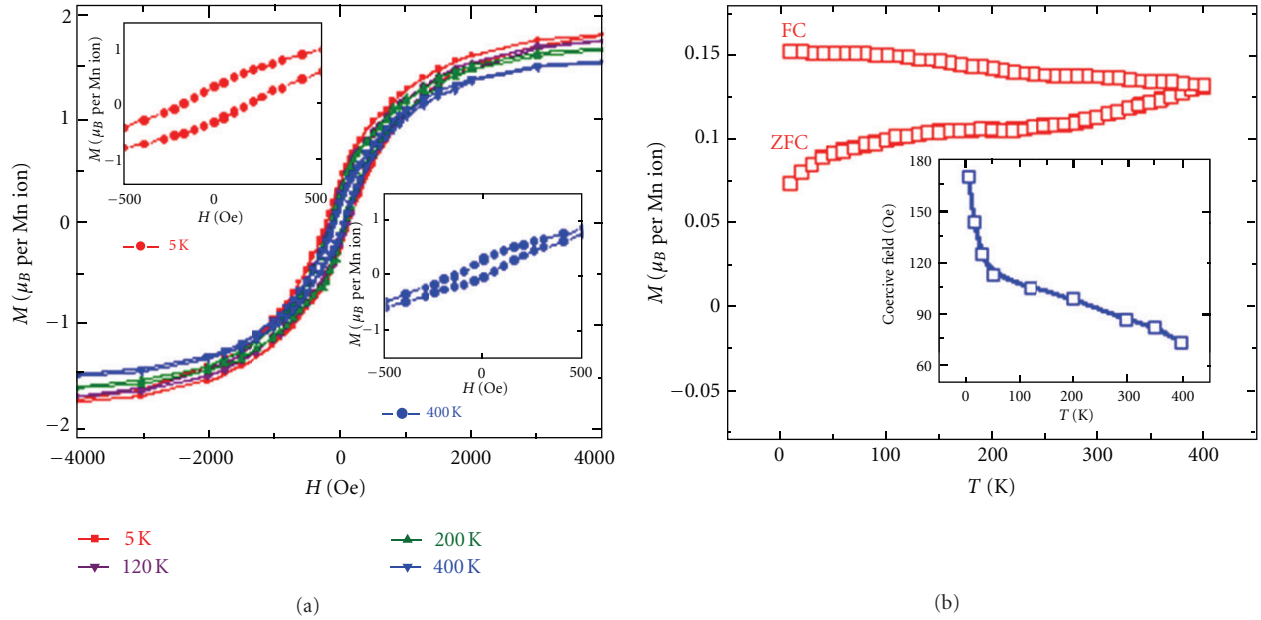

FIGURE 14: Magnetic properties of $Mn_{0.05}Ge_{0.95}$ QDs. (a) Hysteresis loops at 5, 120, 200, and 400 K. (b) ZFC and FC magnetization curves under a magnetic field of 100 Oe. Temperature-dependent coercivity is displayed in the inset. Reproduced from [17]. Copyright ©2010, Macmillan Publishers Limited.

mainly associate with the Mn-rich clusters. Typical zero-field cooling-field curves of $Ge_{1-x}Mn_x$ (x = 1%, 4%) film (grown at 70°C and 150°C) have been displayed in Figure 11 [16]. The secondary precipitates are absent in samples with 1% Mn grown at 70°C; coherent clusters may exist according to the ZFC-FC result. As for the samples grown at 150°C, since all the samples are confirmed with the existence of Mn-rich secondary clusters, such as Mn_5Ge_3, their ZFC and FC curves are quite similar.

2.3. Ge-Based Quantum Dots

2.3.1. GeMn Quantum Dots. High Mn concentration is necessary to achieve RT ferromagnetism; however, Mn-rich clusters are almost observed in all of the reported GeMn thin films with a higher Mn concentration (say ~3%). In order to avoid the formation of Mn-rich clusters, GeMn quantum dots (QDs) with normally a height of several nanometers were grown by Mn implantation [46] or MBE [17, 41]. In particular, GeMn QDs may exhibit unique and salient performance resulted from size and quantum confinement effects, affecting carrier transport, spin lifetimes, interactions of spins, and, thus, ferromagnetic properties [47]. In recent work [17, 41], high-T_C self-assembled $Mn_{0.05}Ge_{0.95}$ QDs grown on Si substrates have been successfully fabricated by MBE. High-resolution TEM (Figure 12(a) [17]) reveals that the QD has a dome shape with a base diameter of about 40 nm and a height of about 9 nm. The fast Fourier transformation (Figure 12(b)) and HRTEM image of the MnGe lattice through the Fourier filter (Figure 12(c)) reveal that the dot is single crystalline with no evidence of pronounced dislocations or stacking faults. Moreover, amorphous layers generally associated with Mn oxidation are not found, either. Further structural and magnetic characterizations confirm the formation of single crystalline DMS quantum dots without observable Mn_5Ge_3 or $Mn_{11}Ge_8$ precipitates and the material has a strong ferromagnetism above 400 K.

2.3.2. GeFe Quantum Dots. In order to avoid the formation of cluster of Mn, transition metal Fe was selected as a promising dopant. However, the Curie temperatures obtained from Fe-doped Ge DMS bulk films have been limited to low temperatures [48, 49]. Recently, self-assembled $Fe_{0.02}Ge_{0.98}$ dilute magnetic quantum dots with a high Curie temperature above 400 K have been successfully synthesized [18]. TEM images (Figures 13(a), 13(b)) [18] show that the nanostructure of $Fe_{0.02}Ge_{0.98}$ is similar to that of $Mn_{0.05}Ge_{0.95}$ except for the absence of Fe diffusion into the underlying Si. Fe composition (~2 atom %) was determined by energy-dispersive X-ray (EDX) spectroscopy, and the result is shown in Figure 13(c).

2.3.3. Magnetic Properties. As discussed above, both $Mn_{0.05}Ge_{0.95}$ QDs and $Fe_{0.02}Ge_{0.98}$ QDs show a perfect single crystallinity without any Mn-rich clusters or precipitates. Consequently, different magnetic properties from that of the thin films can be expected. Indeed, it has been demonstrated by the magnetic measurement, as shown in Figure 14 [17]. Hysteresis loops in Figure 14(a) indicate a strong ferromagnetism above 400 K, and consistent conclusion can also be drawn from Figure 14(b) (ZFC-FC results). It should be noted that the wide separation of the ZFC and FC curves in the temperature range of 5 to 400 K shows

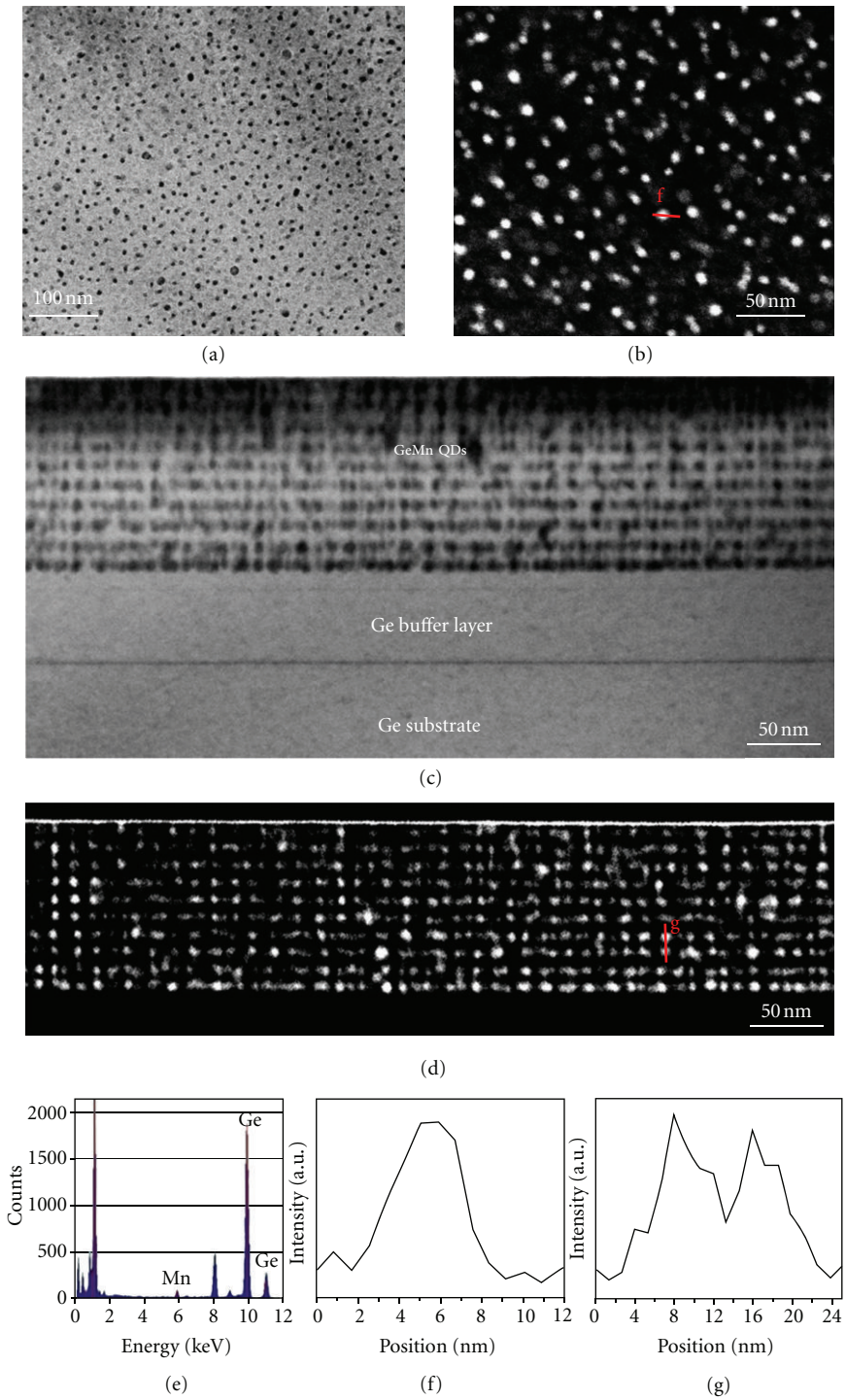

Figure 15: (a) A plane-view bright-field TEM image of MnGe nanodots (dark spots). (b) A plane-view low-angle dark-field STEM image of the MnGe nanodots (white spots). (c) A cross-sectional TEM image of the MnGe nanodot arrays (dark spot arrays). (d) A cross-section STEM image of the MnGe nanodot arrays (white spot arrays). (e) An EDS profile showing the Mn and Ge peaks. ((f), (g)) EDS line-scan profiles of the line marked in (b) and (e) using Mn K peak, respectively. Reproduced from [19]. Copyright ©2011 Wang et al.; licensee Springer [19].

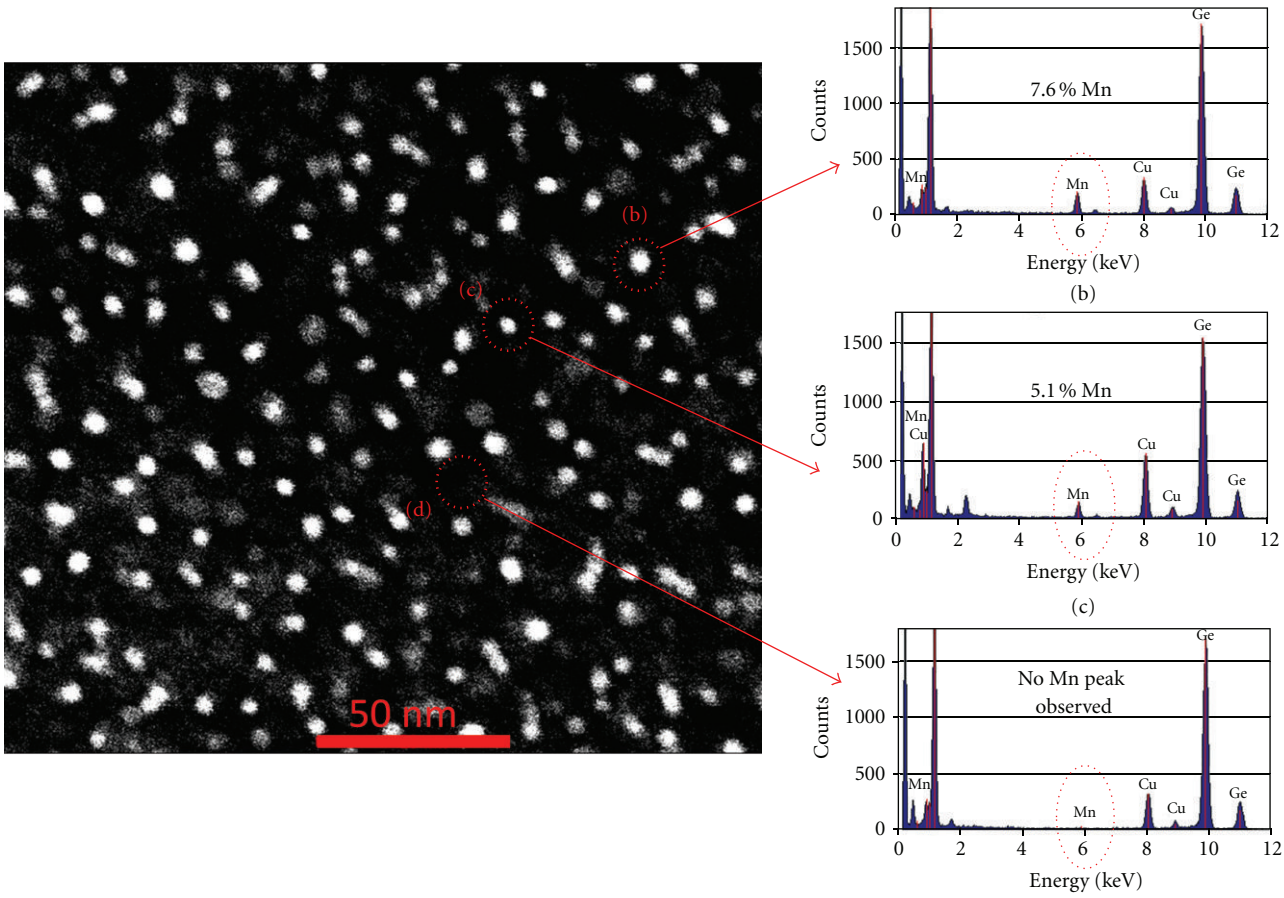

Figure 16: (a) A plane-view dark-field STEM image showing the MnGe nanodots (white spots). ((b)–(d)) EDS profiles showing Mn and Ge peaks and the Mn concentration in the regions marked in (a).

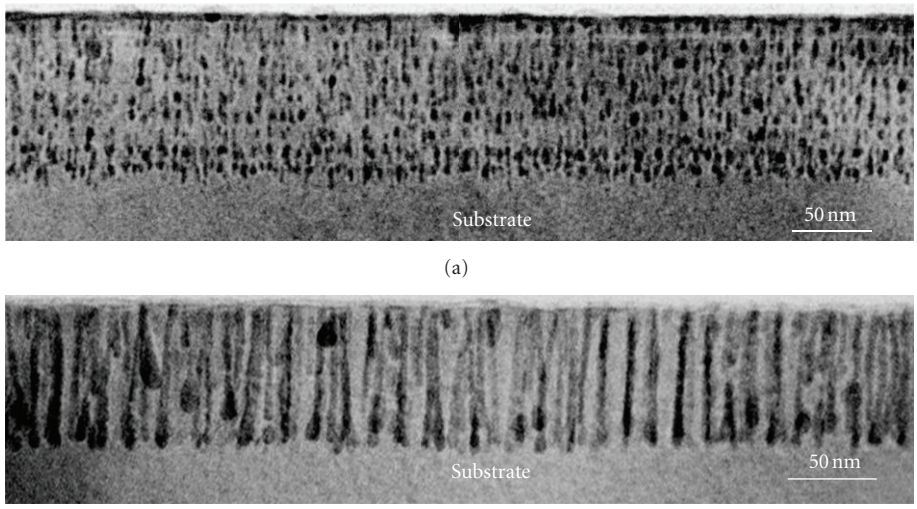

Figure 17: Typical TEM images of samples with different spacer thickness, (a) Ge layer = 11 nm, GeMn layer = 1.2 nm, (b) Ge layer = 4.6 nm, GeMn layer = 3 nm. Reproduced from [20]. Copyright ©2011 Wang et al.; licensee Springer.

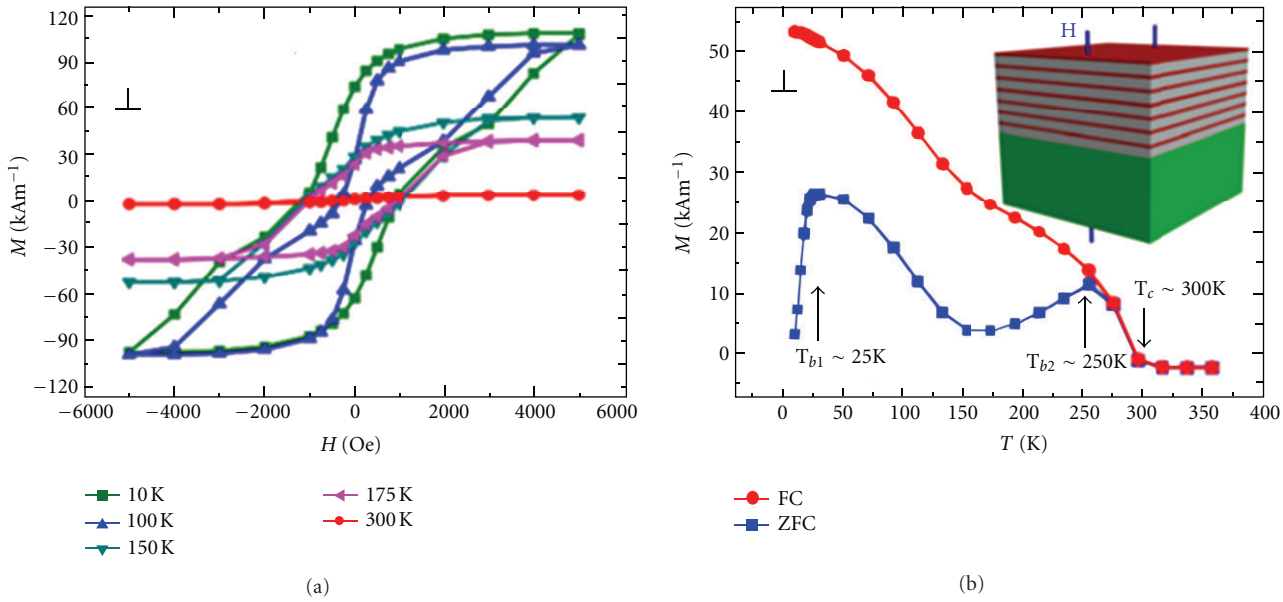

FIGURE 18: Magnetic properties of the MnGe nanowells. (a) Temperature-dependent hysteresis loops at 10, 100, 150, 175, and 300 K, with the sample surface perpendicular to the external magnetic field. (b) ZFC and FC curves under a magnetic field of 200 Oe, and the sample setup during the SQUID measurements (inset). Reproduced from [21]. Copyright ©2010 IOP Publishing Ltd.

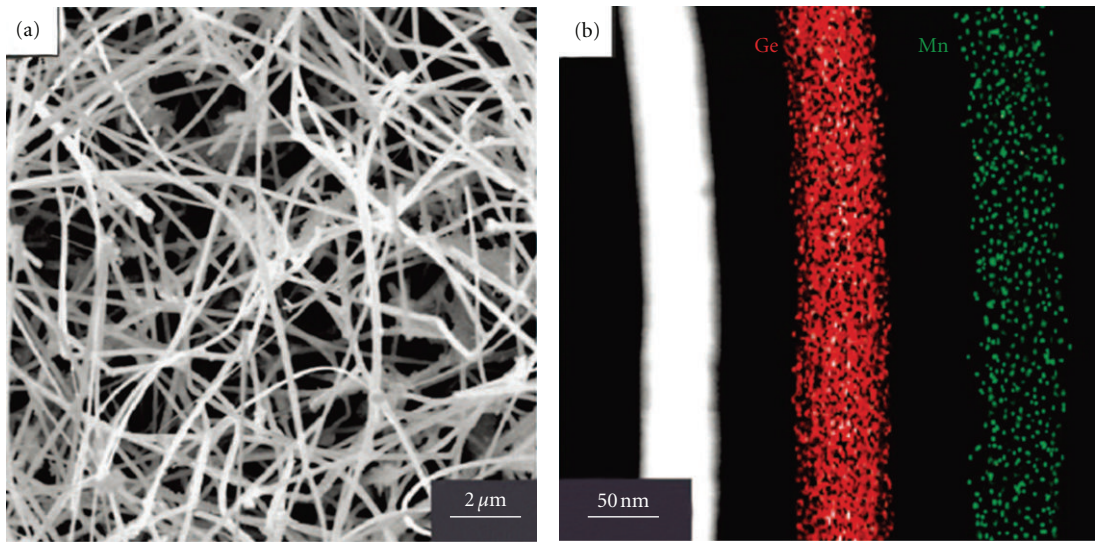

FIGURE 19: (a) SEM images of the $Ge_{0.8}Mn_{0.2}$ NWs and (b) their STEM image and EDX elemental mapping, showing that 20% Mn element is distributed uniformly over the whole NWs. Reproduced from [22]. Copyright ©2008, American Chemical Society.

the irreversibility of susceptibilities, possibly resulting from strain-induced anisotropy attributed to the large lattice mismatch existing between Si and Ge.

2.4. GeMn Ordered Arrays

2.4.1. Morphology and Composition. As illustrated in Figure 8, Mn-rich clusters will occur when the film thickness reaches a threshold at certain growth conditions. Therefore, it is desirable to grow thinner films to avoid Mn-rich precipitates. Using this strategy, other than GeMn QDs mentioned above, GeMn nanodot arrays were successfully fabricated by employing a "superlattice" method [19, 21]. Figures 15(a) and 15(c) [19] are plane-view and cross-sectional TEM images and show the general morphology of the MnGe nanostructures, respectively. A high density of dark nanodots can be clearly seen in both cases. The composition of dark dots is determined by EDS in STEM mode, as shown in Figures 15(b) and 15(d). The results of EDS line scans (marked in Figures 15(b) and 15(d)) using the Mn *K* peak have been displayed in Figures 15(f) and 15(g), indicating high concentration of Mn. Mn concentration of

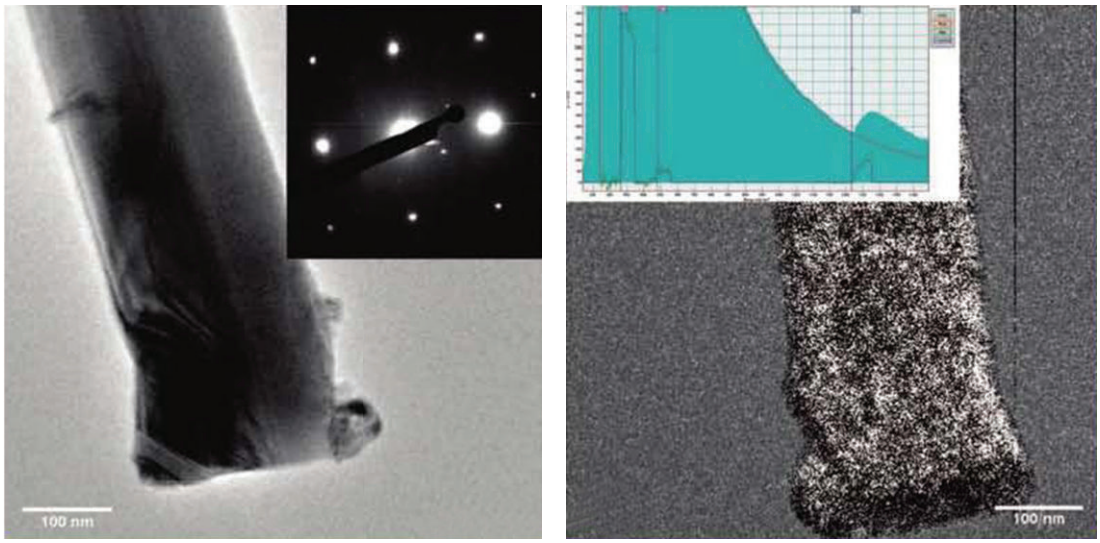

(a) (b)

Figure 20: (a) A bright-field TEM image of a 180 nm GeMn NW. Inset is the electron diffraction pattern of the NW. (b) Mn map of a 180 nm GeMn NW in (a) obtained by EELS mapping. Inset is the EELS spectrum, indicating the presence of the Mn peak at L-edge. Reproduced from [23]. Copyright ©2009 American Chemical Society.

dots has been further quantitatively investigated, and the result is shown in Figure 16, which demonstrates that the nanodots inside are Mn-rich and Mn poor outside.

2.4.2. The Effect of Substrates, Mn Concentration, and Growth Temperature. Growth conditions of the ordered arrays, including substrates, Mn concentration, and growth temperature have been recently systematically explored [20]. It is revealed that GeMn nanodot arrays can be formed ordered on Ge and GaAs substrates at low temperature (~70°C), but disordered on Si, simultaneously companied by a large amount of stacking faults. This can be explained by the fact that the lattice constant of Ge which is 0.5656 nm, close to that of GaAs (0.5653 nm), is larger than that of Si (0.543 nm). Figure 17 [20] shows the effect of Ge/GeMn thickness. It should be noted that less strain coupling from the two adjacent MnGe layers is triggered by larger Ge spacer layer or a narrower MnGe layer, resulting in less ordered MnGe nanodots. In addition to substrate and Ge/GeMn thickness, Mn concentration, as well as growth temperature, also plays an important role in controlling the behavior of GeMn nanostructure. Since higher growth temperature and/or higher Mn concentration lead to the formation of Mn-rich secondary precipitates, there should be an optimal growth temperature and Mn concentration to secure the ordered nanodot arrays [20].

2.4.3. Magnetic Properties. Well-aligned MnGe nanocolumns and nanowells can be successfully fabricated by low-temperature MBE with a Curie temperature up to 300 K, confirmed by the hysteresis loops displayed in Figure 18(a) [21]. In addition, as shown in Figure 18(b), the MnGe nanowells exhibit a substantial difference between the ZFC and FC curves, resulting from the blocking transitions of superparamagnetic particles. Both structural (not mentioned here) and magnetic property measurements indicate the presence of two phases in both nanocolumns and nanowells, the lattice-coherent nanostructures with a low blocking temperature $T_{b1} \sim 25$ K and the Mn_5Ge_3 metallic precipitates with $T_{b2} \sim 250$ K. Moreover, magnetotransport measurements reveal the fact that the nanowells and nanocolumns have positive and negative magnetoresistances, respectively, which can be interpreted by different spin scattering mechanisms under magnetic fields.

2.5. GeMn Nanowires. GeMn wires with low dimensionality on a nanometer scale can easily get rid of the effect of defects or nonuniform distribution of Mn since they have thermodynamically stable features and are typically single crystals with no defects [50]. Currently, two typical methods are extensively employed in fabricating GeMn nanowires (NWs), namely, thermal vapor transport method (TVT) [22, 51] and supercritical fluid-liquid-solid method (SFLS) [23].

2.5.1. Thermal Vapor Transport Method. As illustrated in Figure 19 [22], for GeMn NWs prepared by thermal vapor transport method, Mn even as high as 20% can be distributed homogeneously along the whole nanowires and without any phase separation or spinodal decomposition. However, the field-dependent magnetization shows despite of the capability of 20% Mn doped into Ge matrix, the room-temperature ferromagnetism is maximized at 10%. Moreover, a typical drawback in vapor transport method is the formation of amorphous MnO in the process.

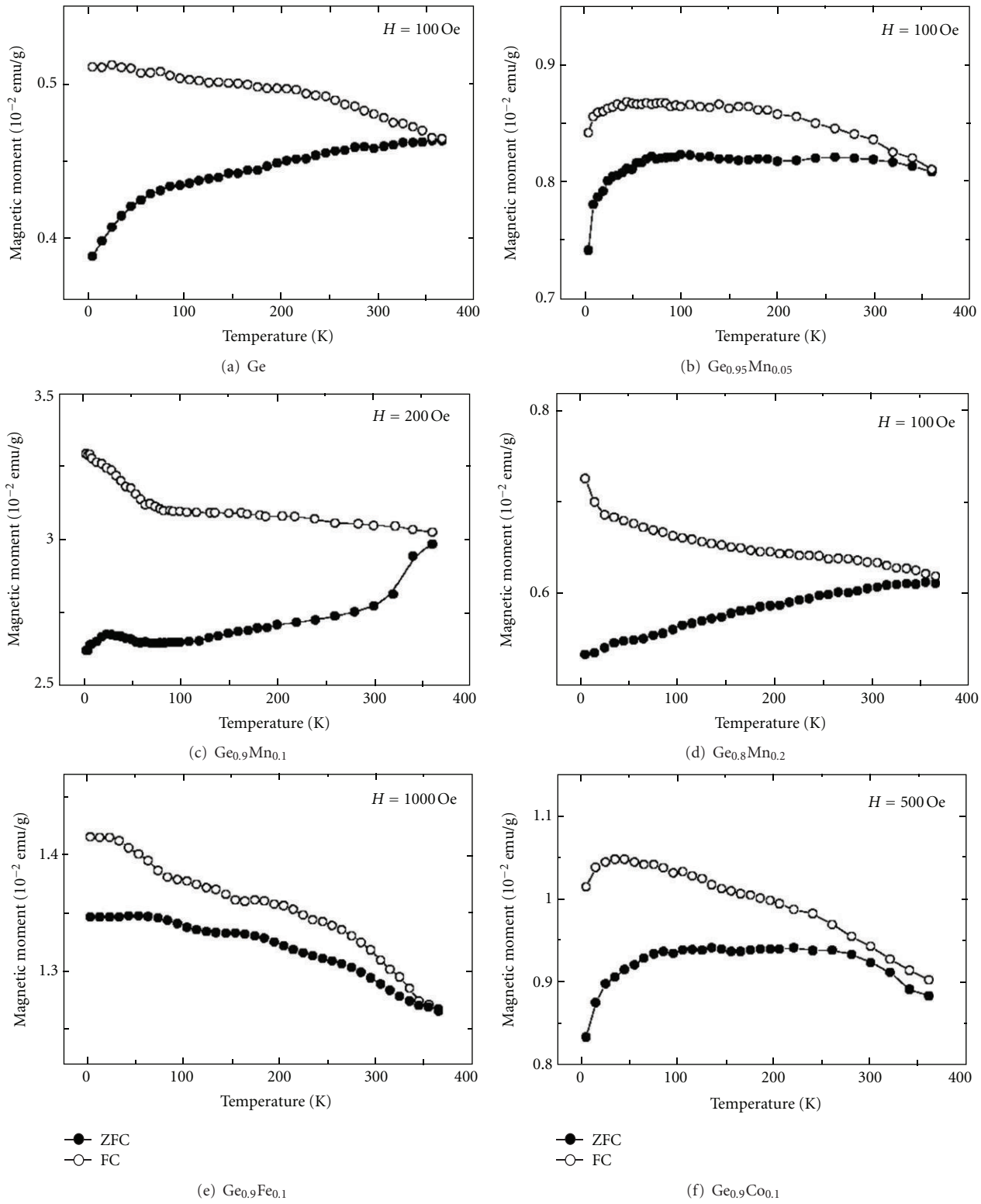

Figure 21: ZFC and FC curves of the (a) Ge, (b) $Ge_{0.95}Mn_{0.05}$, (c) $Ge_{0.9}Mn_{0.1}$, (d) $Ge_{0.8}Mn_{0.2}$, (e) $Ge_{0.9}Fe_{0.1}$, and (f) $Ge_{0.9}Co_{0.1}$ NWs, under a magnetic field at H = 100–1000 Oe, indicating that the ferromagnetism persists to 350 K. Reproduced from the supporting information of [22]. Copyright ©2008, American Chemical Society.

Table 1: Summary of typical $Ge_{1-x}Mn_x$ obtained with various growth methods.

NO.	Growth method	Substrate	Dopant concentration (at.)	T_S (°C)	T_C (K)	Main clusters
1 [5]	Bridgeman method	—	0/0.0044/0.013/0.038/0.062	1050	150–285	None
2 [7, 12]	Bridgeman method	—	0–0.1	1050	150–285	$Mn_{11}Ge_8$, Mn_5Ge_3
3 [10]	Ion implantation	Ge (100)	—	RT-300	—	Mn cluster, Mn_5Ge_3
4 [24]	Ion implantation	Ge (100)	~0.04	240/270	—	Mn_5Ge_3
5 [26]	Ion implantation	Ge (100)	—	300	250–270	Mn_5Ge_3
6 [27]	Ion implantation	Ge (100)	≤0.12	RT	~20	None
7 [13]	Ion implantation	Ge (100)	0.04	LN	5–293	None
8 [30]	Ion implantation	Ge (111)	—	RT	~300	None
9 [4]	MBE	GaAs (001)	0.006–0.035	70	25–166	$Mn_{11}Ge_8$
10 [9]	MBE	Si (001)	0.04	250	—	Mn_5Ge_3
11 [11]	MBE	Ge (100)	0.04	70/120	—	$Mn_{11}Ge_8$, Mn_5Ge_2
12 [31]	MBE	Ge (100)	0.01/0.033/0.05	160	—	Mn_5Ge_3
13 [16]	MBE	Si (001)	0.01–0.04	70/150	—	Mn cluster, $Mn_{11}Ge_8$, Mn_5Ge_3
14 [14]	MBE	Ge (001)	0.025–0.12	70	300	Mn_5Ge_3
15 [15]	MBE	Ge (100)	0.05	60 70–120	<296	None, Mn_5Ge_3
16 [32]	MBE	Ge (100)	0–0.09	50–110	<296	None, Mn_5Ge_3
17 [33]	MBE	Si (001)	0.04	250	~298	Mn_5Ge_3
18 [34]	MBE	Ge (001)	0.01–0.11	80–200	120–170/300/>400	Nanocolumn, Mn_5Ge_3
19 [35]	MBE	Ge (100)	0.01–0.051	160	185–235	—
20 [36]	MBE	Ge (111)	0.03	50	~300	None
21 [37]	MBE	Ge (001)	~0.02	225	~290	Mn_5Ge_3
22 [38]	MBE	GaAs (001)	0.25–0.42	160–300	104	$Mn_{11}Ge_8$, Mn_5Ge_3
23 [39]	MBE	Ge (100)	0.034/0.402	120/70	300	Mn_5Ge_3
24 [40]	MBE	Si (001)	0.04	70	~300	Mn_5Ge_3
25 [17, 41]	MBE	Si (001)	0.05	450	~400	None
26 [21]	MBE	GaAs	—	70	~300	Coherent nanostructure, Mn_5Ge_3
27 [22]	TVT	—	0.05–0.20	800	350	None
28 [23]	SFLS	—	0.005–0.01	450	300	None

2.5.2. Supercritical Fluid-Liquid-Solid Method. An effective way to avoid the thick oxide shell like MnO is SFLS. SFLS growth can be achieved by using pressurized solvents at temperatures exceeding their critical points to produce a wider range of materials, since most semiconductor/metal eutectic temperatures exceed the boiling point of conventional solvents [52]. As illustrated in Figure 20 [23], van der Meulen et al. have successfully fabricated single-crystalline GeMn nanowires with an average Mn concentration of 0.5–1.0%. They reported that Mn atoms occupied substitutional sites and no secondary phases were observed.

2.5.3. Magnetic Properties. The field-cooled (FC) and zero-field-cooled (ZFC) magnetic moment versus temperature (M_{FC} and M_{ZFC} versus T) curves, shown in Figure 21 [22], clearly indicate that the ferromagnetism persists to 350 K, no matter for Ge, $Ge_{1-x}Mn_x$ ($x = 0.05, 0.1, 0.2$), or $Ge_{0.9}M_{0.1}$ (M = Fe, Co). Surprisingly, the ferromagnetic behaviors of undoped Ge NWs are quite unusual, resulting probably from the surface contribution. Further investigation confirms that the magnetic moment of the $Ge_{1-x}Mn_x$ NWs exhibits a much larger magnetic moment than the undoped Ge NWs and reaches a maximum value at $x = 0.1$. However, the Fe and Co substitutions do not lead to a significant enhancement in magnetic moment, approximately in the same order of magnitude as undoped Ge NWs. Therefore, Mn substitution, compared with Fe and Co substitutions, is considered more promising to produce powerful ferromagnetic Ge NWs [22].

3. Summary and Conclusion

3.1. Summary Table. The microstructures and Curie temperatures of $Ge_{1-x}Mn_x$ obtained with various growth methods are summarized in Table 1, which shows that the most commonly observed Mn clusters are coherent nanostructure, Mn_5Ge_3 and $Mn_{11}Ge_8$.

3.2. Conclusions and Prospects. The research on DMSs has been emphasized in the past 30 years, and this endeavor was fuelled by both progress and problems. Presently, the main challenge remains the growth of an ideal material achieving

ferromagnetism at room temperature and higher. In this paper, the experiment status of the fabrications of bulks, films, QDs, ordered arrays, and nanowires of GeMn DMSs has been presented.

Although tremendous progress has been made on the improvement of growth techniques, coherent Mn-rich clusters and Mn-rich precipitates were generally observed. In order to avoid such Mn-rich clusters formed during MBE growth, substrate temperature, Mn concentration, and film thickness need to be optimized. Among all these improvements, QDs DMS might be the most promising for a spintronic device since it has been demonstrated by ferromagnetism above 400 K with no formation of precipitates.

There is still an awful lot to do before DMSs can be practically used on a large scale, but experimental progress has left several ways open and sketched a promising future.

Acknowledgments

The authors acknowledge the support of the National Science Foundation of China (no. 11174244), National 1000 Young Talents Program of China, and Australian Research Council. Y. Wang would like to acknowledge Faxian Xiu at Iowa State University, Kang L. Wang at University of California Los Angeles, and Jin Zou at University of Queensland for their contribution to this work.

References

[1] M. N. Baibich, J. M. Broto, A. Fert et al., "Giant magnetoresistance of (001)Fe/(001)Cr magnetic superlattices," *Physical Review Letters*, vol. 61, no. 21, pp. 2472–2475, 1988.

[2] S. A. Wolf, D. D. Awschalom, R. A. Buhrman et al., "Spintronics: a spin-based electronics vision for the future," *Science*, vol. 294, no. 5546, pp. 1488–1495, 2001.

[3] Y. D. Park, A. Wilson, A. T. Hanbicki et al., "Magnetoresistance of Mn:Ge ferromagnetic nanoclusters in a diluted magnetic semiconductor matrix," *Applied Physics Letters*, vol. 78, no. 18, pp. 2739–2741, 2001.

[4] Y. D. Park, A. T. Hanbicki, S. C. Erwin et al., "A group-IV ferromagnetic semiconductor: Mn_xGe_{1-x}," *Science*, vol. 295, no. 5555, pp. 651–654, 2002.

[5] S. Cho, S. Choi, S. C. Hong et al., "Ferromagnetism in Mn-doped Ge," *Physical Review B*, vol. 66, no. 3, Article ID 033303, 3 pages, 2002.

[6] A. Stroppa, S. Picozzi, A. Continenza, and A. J. Freeman, "Electronic structure and ferromagnetism of Mn-doped group-IV semiconductors," *Physical Review B*, vol. 68, no. 15, Article ID 155203, 9 pages, 2003.

[7] E. Biegger, L. Stäheli, M. Fonin, U. Rüdiger, and Y. S. Dedkov, "Intrinsic ferromagnetism versus phase segregation in Mn-doped Ge," *Journal of Applied Physics*, vol. 101, no. 10, Article ID 103912, 5 pages, 2007.

[8] T. Dietl, "A ten-year perspective on dilute magnetic semiconductors and oxides," *Nature Materials*, vol. 9, no. 12, pp. 965–974, 2010.

[9] Y. Wang, J. Zou, Z. Zhao, X. Han, X. Zhou, and K. L. Wang, "Mn behavior in Ge0.96 Mn0.04 magnetic thin films grown on Si," *Journal of Applied Physics*, vol. 103, no. 6, Article ID 066104, 3 pages, 2008.

[10] L. Ottaviano, M. Passacantando, A. Verna et al., "Microscopic investigation of the structural and electronic properties of ion implanted Mn-Ge alloys," *Physica Status Solidi (A) Applications and Materials*, vol. 204, no. 1, pp. 136–144, 2007.

[11] Y. Wang, J. Zou, Z. Zhao, X. Han, X. Zhou, and K. L. Wang, "Direct structural evidences of $Mn_{11}Ge_8$ and Mn_5Ge_2 clusters in $Ge_{0.96}Mn_{0.04}$ thin films," *Applied Physics Letters*, vol. 92, no. 10, Article ID 101913, 3 pages, 2008.

[12] J.-S. Kang, G. Kim, S. C. Wi et al., "Spatial chemical inhomogeneity and local electronic structure of Mn-doped Ge ferromagnetic semiconductors," *Physical Review Letters*, vol. 94, no. 14, Article ID 147202, 4 pages, 2005.

[13] L. Ottaviano, A. Continenza, G. Profeta et al., "Room-temperature ferromagnetism in Mn-implanted amorphous Ge," *Physical Review B*, vol. 83, no. 13, Article ID 134426, 9 pages, 2011.

[14] Y. Wang, F. Xiu, Y. Wang et al., "Mn-rich clusters in GeMn magnetic semiconductors: structural evolution and magnetic property," *Journal of Alloys and Compounds*, vol. 508, no. 2, pp. 273–277, 2010.

[15] S. Ahlers, D. Bougeard, N. Sircar et al., "Magnetic and structural properties of Ge_xMn_{1-x} films: precipitation of intermetallic nanomagnets," *Physical Review B*, vol. 74, no. 21, Article ID 214411, 8 pages, 2006.

[16] Y. Wang, Y. Wang, F. Xiu et al., "Effect of Mn concentration and growth temperature on nanostructures and magnetic properties of $Ge_{1-x}Mn_x$ grown on Si," *Journal of Crystal Growth*, vol. 312, no. 20, pp. 3034–3039, 2010.

[17] F. Xiu, Y. Wang, J. Kim et al., "Electric-field-controlled ferromagnetism in high-Curie-temperature $Mn_{0.05}Ge_{0.95}$ quantum-dots," *Nature Materials*, vol. 9, no. 4, pp. 337–344, 2010.

[18] F. Xiu, Y. Wang, X. Kou et al., "Synthesis of high-curie-temperature $Fe_{0.02}Ge_{0.98}$ quantum dots," *Journal of the American Chemical Society*, vol. 132, no. 33, pp. 11425–11427, 2010.

[19] Y. Wang, F. Xiu, Y. Wang et al., "Coherent magnetic semiconductor nanodot arrays," *Nanoscale Research Letters*, vol. 6, no. 1, pp. 1–8, 2011.

[20] Y. Wang, Z. Liao, H. Xu et al., "Structural evolution of GeMn/Ge superlattices grown by molecular beam epitaxy under different growth conditions," *Nanoscale Research Letters*, vol. 6, article 624, 2011.

[21] F. Xiu, Y. Wang, K. Wong et al., "MnGe magnetic nanocolumns and nanowells," *Nanotechnology*, vol. 21, no. 25, Article ID 255602, 2010.

[22] Y. J. Cho, C. H. Kim, H. S. Kim et al., "Ferromagnetic $Ge_{1-x}M_x$ (M = Mn, Fe, and Co) nanowires," *Chemistry of Materials*, vol. 20, no. 14, pp. 4694–4702, 2008.

[23] M. I. van der Meulen, N. Petkov, M. A. Morris et al., "Single crystalline $Ge_{1-x}Mn_x$ nanowires as building blocks for nanoelectronics," *Nano Letters*, vol. 9, no. 1, pp. 50–56, 2009.

[24] L. Ottaviano, M. Passacantando, A. Verna et al., "Direct structural evidences of Mn dilution in Ge," *Journal of Applied Physics*, vol. 100, no. 6, Article ID 063528, 4 pages, 2006.

[25] L. Ottaviano, A. Verna, V. Grossi et al., "Surface morphology of Mn^+ implanted Ge(1 0 0): a systematic investigation as a function of the implantation substrate temperature," *Surface Science*, vol. 601, no. 13, pp. 2623–2627, 2007.

[26] M. Passacantando, L. Ottaviano, F. D'Orazio et al., "Growth of ferromagnetic nanoparticles in a diluted magnetic semiconductor obtained by Mn^+ implantation on Ge single crystals," *Physical Review B*, vol. 73, no. 19, Article ID 195207, 5 pages, 2006.

[27] A. Verna, L. Ottaviano, M. Passacantando et al., "Ferromagnetism in ion implanted amorphous and nanocrystalline

Mn_xGe_{1-x}," *Physical Review B*, vol. 74, no. 8, Article ID 085204, 2 pages, 2006.

[28] D. Bürger, S. Zhou, M. Höwler et al., "Hysteretic anomalous Hall effect in a ferromagnetic, Mn-rich Ge:Mn nanonet," *Applied Physics Letters*, vol. 100, no. 1, Article ID 012406, 4 pages, 2012.

[29] W. Yin, L. He, M. C. Dolph, J. Lu, R. Hull, and S. A. Wolf, "Modulation of the magnetism in ion implanted Mn_xGe_{1-x} thin films by rapid thermal anneal," *Journal of Applied Physics*, vol. 108, no. 9, Article ID 093919, 6 pages, 2010.

[30] L. Lifeng, C. Nuofu, C. Chenlong, L. Yanli, Y. Zhigang, and Y. Fei, "Magnetic properties of Mn-implanted n-type Ge," *Journal of Crystal Growth*, vol. 273, no. 1-2, pp. 106–110, 2004.

[31] J. P. Ayoub, L. Favre, I. Berbezier, A. Ronda, L. Morresi, and N. Pinto, "Morphological and structural evolutions of diluted $Ge_{1-x}Mn_x$ epitaxial films," *Applied Physics Letters*, vol. 91, no. 14, Article ID 141920, 3 pages, 2007.

[32] A. P. Li, J. F. Wendelken, J. Shen, L. C. Feldman, J. R. Thompson, and H. H. Weitering, "Magnetism in Mn_xGe_{1-x} semiconductors mediated by impurity band carriers," *Physical Review B*, vol. 72, no. 19, Article ID 195205, 9 pages, 2005.

[33] M. Ogawa, X. Han, Z. Zhao, Y. Wang, K. L. Wang, and J. Zou, "Mn distribution behaviors and magnetic properties of GeMn films grown on Si (0 0 1) substrates," *Journal of Crystal Growth*, vol. 311, no. 7, pp. 2147–2150, 2009.

[34] T. Devillers, M. Jamet, A. Barski et al., "Structure and magnetism of self-organized $Ge_{1-x}Mn_x$ nanocolumns on Ge(001)," *Physical Review B*, vol. 76, no. 20, Article ID 205306, 12 pages, 2007.

[35] N. Pinto, L. Morresi, M. Ficcadenti et al., "Magnetic and electronic transport percolation in epitaxial $Ge_{1-x}Mn_x$ films," *Physical Review B*, vol. 72, no. 16, Article ID 165203, 7 pages, 2005.

[36] R. Gunnella, L. Morresi, N. Pinto et al., "Magnetization of epitaxial MnGe alloys on Ge(1 1 1) substrates," *Surface Science*, vol. 577, no. 1, pp. 22–30, 2005.

[37] C. Bihler, C. Jaeger, T. Vallaitis et al., "Structural and magnetic properties of Mn_5Ge_3 clusters in a dilute magnetic germanium matrix," *Applied Physics Letters*, vol. 88, no. 11, Article ID 112506, 3 pages, 2006.

[38] H. Li, Y. Wu, Z. Guo, P. Luo, and S. Wang, "Magnetic and electrical transport properties of $Ge_{1-x}Mn_x$ thin films," *Journal of Applied Physics*, vol. 100, no. 10, Article ID 103908, 9 pages, 2006.

[39] S. Ahlers, D. Bougeard, H. Riedl et al., "Ferromagnetic Ge(Mn) nanostructures," *Physica E*, vol. 32, no. 1-2, pp. 422–425, 2006.

[40] J. Zou, Y. Wang, F. Xiu, K. L. Wang, and A. P. Jacob, "Tadpole shaped $Ge_{0.96}Mn_{0.04}$ magnetic semiconductors grown on Si," *Applied Physics Letters*, vol. 96, no. 5, Article ID 051905, 3 pages, 2010.

[41] F. Xiu, I. V. Ovchinnikov, P. Upadhyaya et al., "Voltage-controlled ferromagnetic order in MnGe quantum dots," *Nanotechnology*, vol. 21, no. 37, Article ID 375606, 2010.

[42] V. Ko, K. L. Teo, T. Liew et al., "Correlation of structural and magnetic properties of ferromagnetic Mn-implanted $Si_{1-x}Ge_x$ films," *Journal of Applied Physics*, vol. 103, no. 5, Article ID 053912, 7 pages, 2008.

[43] W. Zhu, H. H. Weitering, E. G. Wang, E. Kaxiras, and Z. Zhang, "Contrasting growth modes of Mn on Ge(100) and Ge(111) surfaces: subsurface segregation versus intermixing," *Physical Review Letters*, vol. 93, no. 12, Article ID 126102, 4 pages, 2004.

[44] Y. Wang, Z. M. Zeng, X. F. Han, X. G. Zhang, X. C. Sun, and Z. Zhang, "Temperature-dependent Mn-diffusion modes in CoFeB- and CoFe-based magnetic tunnel junctions: electron-microscopy studies," *Physical Review B*, vol. 75, no. 21, Article ID 214424, 4 pages, 2007.

[45] M. Jamet, A. Barski, T. Devillers et al., "High-curie-temperature ferromagnetism in self-organized $Ge_{1-x}Mn_x$ nanocolumns," *Nature Materials*, vol. 5, no. 8, pp. 653–659, 2006.

[46] J. Chen, K. L. Wang, and K. Galatsis, "Electrical field control magnetic phase transition in nanostructured Mn_xGe_{1-x}," *Applied Physics Letters*, vol. 90, no. 1, Article ID 012501, 3 pages, 2007.

[47] R. Knobel, N. Samarth, S. A. Crooker, and D. D. Awschalom, "Spin-polarized quantum transport and magnetic field-dependent carrier density in magnetic two-dimensional electron gases," *Physica E*, vol. 6, no. 1, pp. 786–789, 2000.

[48] Y. Shuto, M. Tanaka, and S. Sugahara, "Magneto-optical properties of group-IV ferromagnetic semiconductor $Ge_{1-x}Fe_x$ grown by low-temperature molecular beam epitaxy," *Journal of Applied Physics*, vol. 99, no. 8, Article ID 08D516, 3 pages, 2006.

[49] Y. Shuto, M. Tanaka, and S. Sugahara, "Structural and magnetic properties of epitaxially grown $Ge_{1-x}Fe_x$ thin films: fe concentration dependence," *Applied Physics Letters*, vol. 90, no. 13, Article ID 132512, 3 pages, 2007.

[50] U. Kim, T. E. Park, I. Kim et al., "Magnetic anisotropy in vertically aligned diluted magnetic Mn:Ge semiconductor nanowires," *Journal of Applied Physics*, vol. 106, no. 12, Article ID 123903, 4 pages, 2009.

[51] V. Grossi, P. Parisse, M. Passacantando et al., "Surface chemistry study of Mn-doped germanium nanowires," *Applied Surface Science*, vol. 254, no. 24, pp. 8093–8097, 2008.

[52] F. M. Davidson, R. Wiacek, and B. A. Korgel, "Supercritical fluid-liquid-solid synthesis of gallium phosphide nanowires," *Chemistry of Materials*, vol. 17, no. 2, pp. 230–233, 2005.